

Freeform reflectors for architectural lighting

Ruidong Zhu,¹ Qi Hong,¹ Hongxia Zhang,² and Shin-Tson Wu^{1,*}

¹CREOL, The College of Optics and Photonics, University of Central Florida, Orlando, Florida 32816, USA
²College of Precision Instrument and Optoelectronics Engineering, Tianjin University, Tianjin, 300072, China
*swu@ucf.edu

Abstract: We propose an improved method to design freeform reflectors for architectural lighting: one for accent lighting and another for large area wall washing. The designed freeform reflectors effectively distribute light fluxes over the target surfaces, and generate appropriate illumination patterns for comfortable visual environments, which provides greater flexibility for lighting designs, allows many challenging designs, and improves energy-efficiency simultaneously.

©2015 Optical Society of America

OCIS codes: (220.2945) Illumination design; (220.0220) Optical design and fabrication; (080.4298) Nonimaging optics.

References and links

1. J. C. Miñano, P. Benítez, P. Zamora, M. Buljan, R. Mohedano, and A. Santamaría, “Free-form optics for Fresnel-lens-based photovoltaic concentrators,” *Opt. Express* **21**(3), A494–A502 (2013).
2. J. C. Miñano and J. C. González, “New method of design of nonimaging concentrators,” *Appl. Opt.* **31**(16), 3051–3060 (1992).
3. I. Moreno, M. Avendaño-Alejo, and R. I. Tzonchev, “Designing light-emitting diode arrays for uniform near-field irradiance,” *Appl. Opt.* **45**(10), 2265–2272 (2006).
4. K. Wang, D. Wu, Z. Qin, F. Chen, X. Luo, and S. Liu, “New reversing design method for LED uniform illumination,” *Opt. Express* **19**(S4), A830–A840 (2011).
5. R. Zhu, Q. Hong, Y. Gao, Z. Luo, S.-T. Wu, M.-C. Li, S.-L. Lee, and W.-C. Tsai, “Tailoring the light distribution of liquid crystal display with freeform engineered diffuser,” *Opt. Express* **23**(11), 14070–14084 (2015).
6. X. Hu and H. Hua, “High-resolution optical see-through multi-focal-plane head-mounted display using freeform optics,” *Opt. Express* **22**(11), 13896–13903 (2014).
7. E. Chen, R. Wu, and T. Guo, “Design a freeform microlens array module for any arbitrary-shape collimated beam shaping and color mixing,” *Opt. Commun.* **321**(0), 78–85 (2014).
8. F. R. Fournier, W. J. Cassarly, and J. P. Rolland, “Fast freeform reflector generation usingsource-target maps,” *Opt. Express* **18**(5), 5295–5304 (2010).
9. Z. Feng, Y. Luo, and Y. Han, “Design of LED freeform optical system for road lighting with high luminance/illuminance ratio,” *Opt. Express* **18**(21), 22020–22031 (2010).
10. G. Steffy, *Architectural Lighting Design* (Wiley, 2008).
11. R. Whitehead, *Residential Lighting: A Practical Guide* (Wiley, 2004).
12. D. Phillips, *Lighting in Architectural Lighting* (McGraw-Hill, 1964).
13. C. Canavesi, W. J. Cassarly, and J. P. Rolland, “Observations on the linear programming formulation of the single reflector design problem,” *Opt. Express* **20**(4), 4050–4055 (2012).
14. J.-J. Chen, “Freeform surface design for a light-emitting diode-based collimating lens,” *Opt. Eng.* **49**(9), 093001 (2010).
15. R. Wu, L. Xu, P. Liu, Y. Zhang, Z. Zheng, H. Li, and X. Liu, “Freeform illumination design: A nonlinear boundary problem for the elliptic Monge-Ampère equation,” *Opt. Lett.* **38**(2), 229–231 (2013).
16. C. Canavesi, W. J. Cassarly, and J. P. Rolland, “Target flux estimation by calculating intersections between neighboring conic reflector patches,” *Opt. Lett.* **38**(23), 5012–5015 (2013).
17. D. Michaelis, P. Schreiber, and A. Bräuer, “Cartesian oval representation of freeform optics in illumination systems,” *Opt. Lett.* **36**(6), 918–920 (2011).
18. S. A. Kochengin and V. Oliker, “Determination of reflector surfaces from near-field scattering data,” *Inverse Probl.* **13**(2), 363–373 (1997).
19. T. Glimm and V. Oliker, “Optical design of single reflector systems and the Monge-Kantorovich mass transfer problem,” *J. Math. Sci.* **117**(3), 4096–4108 (2003).
20. V. Oliker, “Mathematical aspects of design of beam shaping surfaces in geometrical optics,” in *Trends in Nonlinear Analysis* (Springer, 2003), pp. 193–224.
21. F. R. Fournier, W. J. Cassarly, and J. P. Rolland, “Designing freeform reflectors for extended sources,” *Proc. SPIE* **7423**, 742302 (2009).

22. O. Marinescu and F. Bociort, "Network search method in the design of extreme ultraviolet lithographic objectives," *Appl. Opt.* **46**(35), 8385–8393 (2007).
23. V. Oliker, "Freeform optical systems with prescribed irradiance properties in near-field," *Proc. SPIE* **6342**, 634211 (2006).
24. P. Dutré, P. Bekaert, and K. Bala, *Advanced Global Illumination*, 2nd ed. (A K Peters/CRC Press, F.L., 2006).
25. D. G. Koch, "Simplified irradiance/illuminance calculations in optical systems," *Proc. SPIE* **1780**, 226–240 (1993).
26. R. J. Koschel, *Illumination Engineering: Design with Nonimaging Optics* (Wiley, 2012).
27. R. Wester, G. Müller, A. Völl, M. Berens, J. Stollenwerk, and P. Loosen, "Designing optical free-form surfaces for extended sources," *Opt. Express* **22**(S2 Suppl 2), A552–A560 (2014).
28. R. Wu, Y. Qin, H. Hua, Y. Meuret, P. Benítez, and J. C. Miñano, "Prescribed intensity design for extended sources in three-dimensional rotational geometry," *Opt. Lett.* **40**(9), 2130–2133 (2015).

1. Introduction

Freeform optics have been widely used in solar concentrators [1, 2], display systems [3–6], and illumination applications [7–9] because of its versatility and exceptional performance. Among them, using freeform optics for architectural lighting is of vital importance because a successful lighting not only helps people to see comfortably and effectively, but also promotes an appropriate visual environment. Sufficient luminance intensity allows people to see clearly, high contrast helps attract attention, non-uniform illumination on the wall offers the sense of relaxation, and applying higher luminance more uniformly to the wall enhances the impression of spaciousness [10–12]. Roughly speaking, there are two main types of freeform components used for architectural lighting: 1) the freeform reflector [8, 13], which uses the law of reflection, and 2) the freeform lens [14–17] which uses both refraction and total internal reflection. Although both approaches can achieve exceptional results, freeform reflector is sometimes preferred due to its negligible chromatic aberration.

In this paper, we develop an improved method for designing freeform reflectors based on the supporting ellipsoid approach [18, 19]. We have modified the intersection calculation method [16, 20] to improve the speed and accuracy of the reflector generation process. Meanwhile, we have also developed the average calculation method to simplify the process of surface representation. After explaining the design method, we apply our freeform reflector to two architectural lighting cases: one for accent lighting and another for large area uniform wall washing. Our promising results suggest that freeform reflectors have great potential applications in architectural lighting.

2. Design method

2.1 Determination of ellipsoid patches

Here, we elucidate our design of freeform reflector using the supporting ellipsoid approach, which is based on the point source assumption. The detailed design approach can be explained as follows: first, the task area is divided into $N_x \times N_y$ meshes and then each mesh is assigned with predetermined illuminance to meet the desired illumination pattern (uniform, Gaussian, etc.). Each task mesh corresponds to a reflecting ellipsoid whose optical property is that light coming from one of the foci will be reflected to the other focus. For the mesh i^{th} in x direction and j^{th} in y direction, we can create such an ellipsoid that one focal point is at the origin O and the other is on the mesh center m_{ij} . The distance between the origin and the mesh center is the focal distance f_{ij} . Mathematically this ellipsoid can be described as [19]:

$$\rho(\mathbf{m}) = \frac{a^2 - c^2}{a - c\mathbf{m} \cdot \hat{\mathbf{v}}}, \quad (1)$$

here a is the semi-axis, c is one half of the focal distance f , \mathbf{m} is the unit vector at the polar angle θ and azimuthal angle φ , and $\hat{\mathbf{v}} = \mathbf{v} / |\mathbf{v}|$ is the unit vector joining two foci. Totally, there are $N_x \times N_y$ ellipsoids, and these ellipsoids partially overlap because they have the origin as their common focal point. As depicted in Fig. 1, to define a crossing reflector, the first

ellipsoid surface intersecting the light ray reflects the light [21]. The final reflector combines a portion of every ellipsoid; each piece belongs to the ellipsoid closest to the origin in that direction. The surface area of an ellipsoid piece determines the amount of luminous flux that it collects. The combination of all ellipsoid pieces determines the final light distribution pattern.

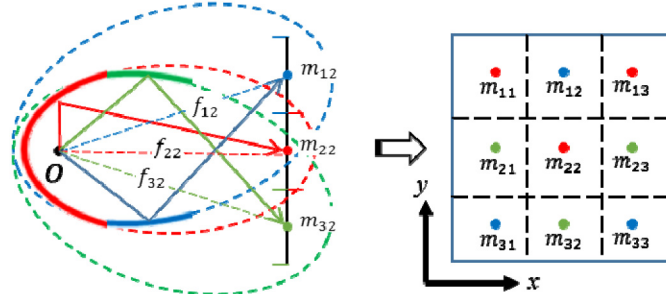


Fig. 1. Task area is divided into N_x and N_y rectangular meshes. Each mesh has a corresponding ellipsoid with one focal point on the origin O and the other on the mesh center m_{ij} . In any direction, the first ellipsoid surface intersecting the light ray reflects the light. The entire reflector combines a portion of every ellipsoid, and each piece belongs to the ellipsoid, which is the closest to the origin in that direction. The surface area of the ellipsoid piece determines the amount of flux that it collects.

As discussed above, determining the semi-axis a of the ellipsoids is the key to the reflector design, and there are two kinds of iterative algorithms to determine them: the adaptive approach and the Olikier's algorithms. The adaptive approach is based on global optimization algorithms such as the least square optimization and the genetic algorithm [22]. This kind of approach usually has fast converging speed but there is no guarantee that it will converge to the global minimum. The Olikier's algorithm has slower converging speed; however, it guarantees that the solution will converge to the global minimum. In this sense, we will use the Olikier's algorithm to generate the reflectors. The detailed approach is outlined as follows: A) Setting the initial parameters: To define a crossing reflector, the initial parameters should be set such that all the flux is collected by the reference ellipsoid. Thus, the semi-axis of all the other ellipsoids is set to the maximum value (except for the reference ellipsoid) [23]:

$$d_{ij} = \frac{2d_0}{1 - \alpha_0 \left(\sqrt{1 + \frac{d_0^2}{F^2}} - \frac{d_0}{F} \right)}. \quad (2)$$

In Eq. (2), $d_{ij} = (a^2 - c^2)/a$ is the focal parameter of the ellipsoids, and d_0 is the focal parameter of the reference ellipsoid. $\alpha_0 = \max(\mathbf{m} \cdot \hat{\mathbf{v}}_0)$ is the maximum value of the scalar product between the unit vector \mathbf{m} and the unit vector $\hat{\mathbf{v}}_0$ over the collection angle. B) Iterative scaling the parameters: After the initial parameters are set, except for the reference ellipsoid, the focal parameter of the ellipsoids are scaled down iteratively to meet the desired illuminance distribution. This process is the famous Olikier's algorithm. The process can be summarized in four steps: 1) Set the increment $\Delta d_{ij} = d_{ij}/3$. 2) Set focal parameters $d_{ij} = d_{ij} - \Delta d_{ij}$. 3) Evaluate the illuminance distribution S_{ij} based on the new focal parameters. 4) Based on the target illuminance distribution T_{ij} , if for all the ellipsoids (excluding the reference ellipsoid) $S_{ij} < T_{ij}$, then go back to step 1 and continue the iteration. If $S_{ij} > T_{ij}$, halve the increment $\Delta d_{ij} = \Delta d_{ij}/2$, set the focal parameters to $d_{ij} = d_{ij} + \Delta d_{ij}$, and then go back to step 3.

With Olikier's algorithm, the illuminance distribution will converge towards the targeted distribution until the difference between S_{ij} and T_{ij} is smaller than the stopping criterion. As

Oliker's approach transfers flux from the reference ellipsoid to the other ellipsoids, the main concern is that when the algorithm converges most of the flux is still collected by the reference ellipsoid. In this sense, the stopping criterion u is defined as:

$$u = \max\left(\left|\frac{S_{ij} - T_{ij}}{T_{ij}}\right|\right) < EPS, \quad (3)$$

here EPS is the predetermined stopping value (for example, 5%).

Even though Oliker's algorithm is well established, we have modified the illuminance evaluation process to improve the accuracy and speed of the algorithm by combining Monte Carlo ray tracing with our modified intersection calculation method. The evaluation process is usually done only by Monte Carlo ray tracing only and the main drawback of this approach is that it requires millions of rays to ensure the accuracy [24]. It means that the ray tracing approach is usually time consuming. However, if we look at the illuminance from a Lambertian source with a luminance of L :

$$\begin{aligned} E &= \iint L \cos \theta d\Omega = \iint L \cos \theta \sin \theta d\theta d\phi = L\omega, \\ \omega &= \iint \cos \theta \sin \theta d\theta d\phi, \end{aligned} \quad (4)$$

here Ω is the solid angle and ω is the projected solid angle. From Eq. (4), we can see that for a Lambertian source, the illuminance is proportional to the projected solid angle. As described in [16], the projected solid angle can be estimated by calculating the intersection between adjacent ellipsoids. Moreover, this approach can be modified and extended to non-Lambertian sources [25]. Figure 2(a) is a representation of the projected solid angles of 25×25 sampling ellipsoids over a collection angle of 40° . Each polygon represents the corresponding ellipsoid patch. In addition, the projected solid angle is represented by the area of the polygon. Figure 2(b) is the close-up view of four adjacent ellipsoids. We can determine from it that at the vertex between four adjacent ellipsoids, there are four 3-ellipsoid intersection points. However, only two of them are on the boundary of the ellipsoid patches. While the other two are within the ellipsoids (the green points). As demonstrated in [16], for the worst scenario, $4(N_x-1)(N_y-1)$ calculations have to be done to determine the inner boundaries. This, however, can be simplified if we take a closer look at the adjacent four ellipsoids, as illustrated in Fig. 2(c), the four 3-ellipsoid intersection points are:

- P_1 : the intersection point between ellipsoid patches $m_{i,j}$, $m_{i,j+1}$ and $m_{i+1,j}$,
- P_2 : the intersection point between $m_{i,j}$, $m_{i,j+1}$ and $m_{i+1,j+1}$,
- P_3 : the intersection point between $m_{i,j}$, $m_{i+1,j}$ and $m_{i+1,j+1}$, and
- P_4 : the intersection point between $m_{i+1,j+1}$, $m_{i,j+1}$ and $m_{i+1,j}$.

For the four points, if P_1 is on the boundary of the ellipsoids, then P_4 will definitely be on the boundary of the ellipsoids, whereas P_2 and P_3 will not. This is because logically if P_2 is on the boundary, we will have two points on the "lower" boundary between $m_{i,j}$ and $m_{i,j+1}$. For the two points, one is definitely at the inner side of the other, which contradicts to the definition of boundary. Similar principle can also be applied to P_3 . As for P_4 , if it is not on the ellipsoids boundary, then we cannot determine the upper-left boundary point of $m_{i+1,j+1}$. Base on the abovementioned analysis, the four 3-ellipsoid intersection points calculation can be simplified as follows:

1. To calculate P_1 ;
2. If P_1 is on the boundary, then we just need to calculate P_4 , and P_1 and P_4 are the two points on the ellipsoid patch boundaries;
3. If P_1 is not on the boundary, we have to calculate both P_2 and P_3 , and these two points are on the ellipsoid patch boundaries.

With the simplified approach, we have to calculate only $3(N_x-1)(N_y-1)$ points for the worst scenario to determine the inner boundaries. Such improvement implies that the speed of the intersection calculation method can be further improved.

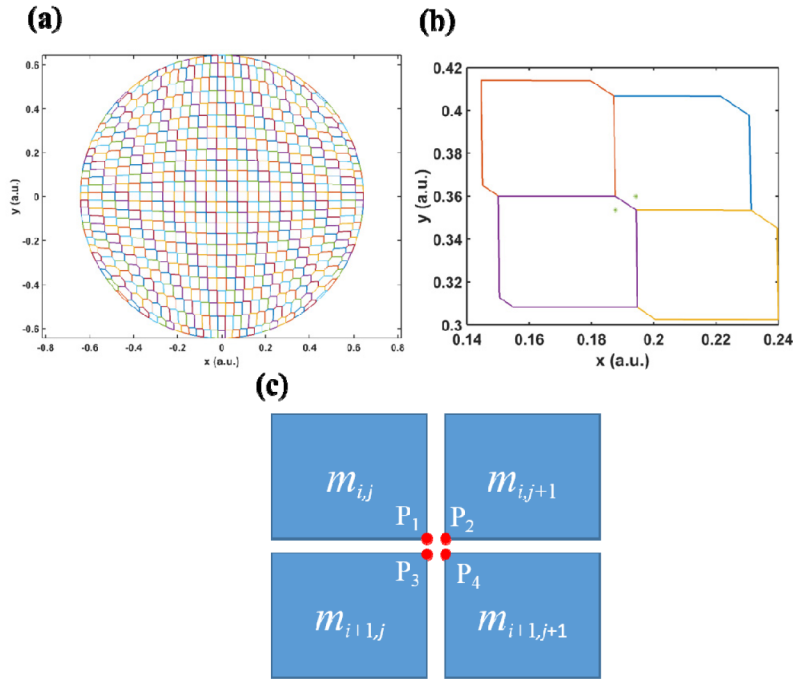


Fig. 2. (a) The projected solid angles of 25×25 ellipsoid patches, (b) the close-up view of four adjacent ellipsoid patches, and (c) the explanation of the four 3-ellipsoid intersection points.

2.2 Surface representation

With Olikier's algorithm, it is possible to determine the ellipsoid patches. However, this is not enough to determine the reflector. As the algorithm is based on the discrete sampling patches, a direct interpretation of the ellipsoid patches will only result in discrete target points instead of a continuous target distribution. Thus, surface smoothing/interpolation is required to ensure the desired target illuminance distribution. There are quite a few approaches for the surface interpolation, such as sampling the reflector along the θ and ϕ direction and the source-task mapping method to generate an integrable reflector [8]. These approaches work extremely well, however, the interpolation process of these approaches have not been fully analyzed. In our approach, we use an average calculation method to determine the reflector. After the ellipsoid patches are determined, each ellipsoid patch is traced with ten-thousand sampled rays, and we can get the intersection points coordinates between the rays and the ellipsoid patch. For the ellipsoid patch m_{ij} , it is represented by the coordinate average of the ten-thousand intersection points (x_{ij}, y_{ij}, z_{ij}) . This coordinate is different from the geometrical center of the ellipsoid as it represents the ray tracing process. The assumption that each ellipsoid patch has to be traced with equal number of rays can be lifted, provided that the source is well sampled. The coordinates of these $N_x \times N_y$ points are imported to LightTools as a freeform surface and then the built-in curvature smoothing feature is applied to reduce the noise. Our results in Section 3 indicate that this approach has a good enough performance.

3. Two design examples

3.1 Freeform reflector for direct lighting

The first design example is a freeform reflector for uniformly illuminating a square area of $3.2\text{m} \times 3.2\text{m}$ located at 3m away from the light source, as Fig. 3(a) depicts. This configuration is typical for direct indoor lighting and street lighting. The reflector, which is located at 10mm away from the light source, has a dimension of $\sim 13\text{mm} \times 13\text{mm} \times 2.5\text{mm}$, and is constructed based on 25×25 ellipsoid patches, as shown in Fig. 3(b). The light source is a Lambertian point source. Over the collection angle of 40° , the freeform reflector can successfully cast the intended light pattern on the target plane, as indicated by Fig. 3(c).

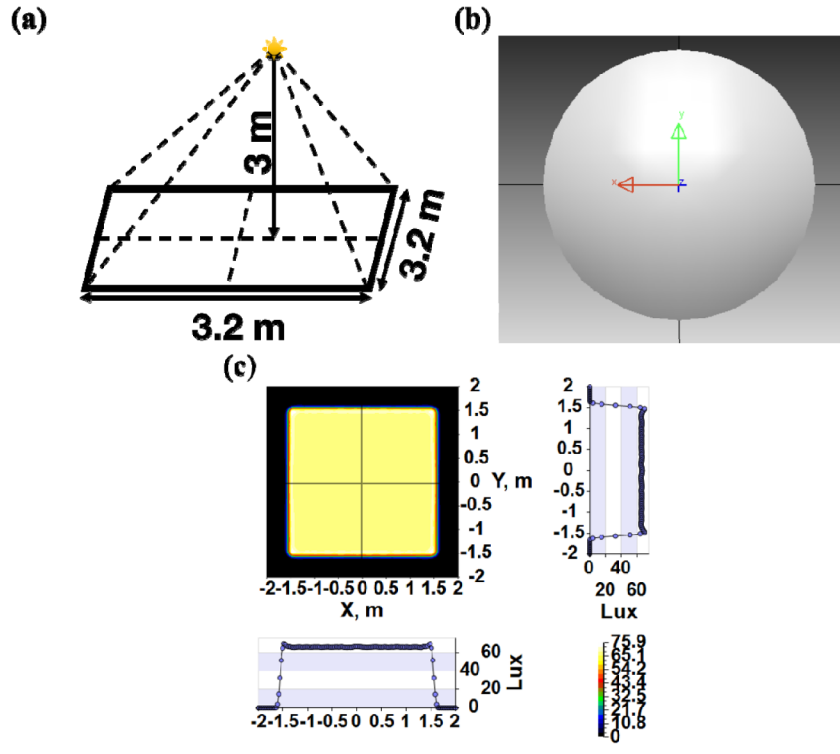


Fig. 3. (a) Illumination configuration of the freeform reflector for direct lighting, (b) the top view of the reflector, and (c) the illuminance distribution on the target plane.

A problem of using freeform reflector for direct lighting is that the light source has to be placed between the reflector and the target plane. In a real world, the light emitting diode (LED) light source is not a point source, and it will definitely block a portion of the light because of the packaging, printed circuit board (PCB), and other mechanical parts. This can be verified by replacing the point source with a real LED source CL-194S-WS, whose packaging is shown in Fig. 4(a). We can see that the mechanical part cannot transmit light and there will be a “hole” in the illumination pattern, as illustrated in Fig. 4(b). A possible solution is to make a hole in the center of the reflector so that the reflected light will not be blocked by the light source. However, this solution usually has to be designed case-by-case based on the real LED geometry, especially when the LED packaging is complex. Thus, it is not preferred to use freeform reflector for direct lighting because of the light blockage.

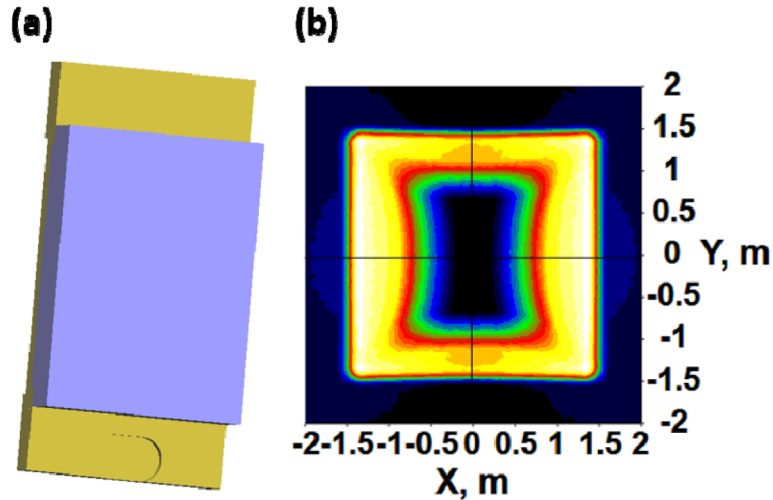


Fig. 4. (a) The packaging of a real LED CL-194S-WS, and (b) the real light illuminance distribution at the target plane because of the light blockage.

3.2 Freeform reflector for wall washing and accent lighting

Without special designs, the emission cones of most available LEDs are nearly hemispherical, which is close to Lambertian radiation pattern. To collect most of the LED light, ideally the freeform reflector should cover LED's entire emission window. However, LED package and PCB as well as LED base that physically holds everything together will block a portion of freeform reflector's aperture, which not only reduces the optical efficiency but also casts a dark shadow on the task plane. To solve this problem, a hemispherical lens is located in front of LED. The planar input surface confines the light into a smaller cone within the critical angle. If the LED is located near the sphere's center, light rays are almost normal to the spherical output surface, so that the light traveling directions are barely changed and the lights are 'condensed' in a smaller emission cone. This allows a gap between LED and the reflector's aperture. The reflector is tilted at an angle for the crossing light ray bundle to pass by LED and the hemispherical lens, as Fig. 5 shows.

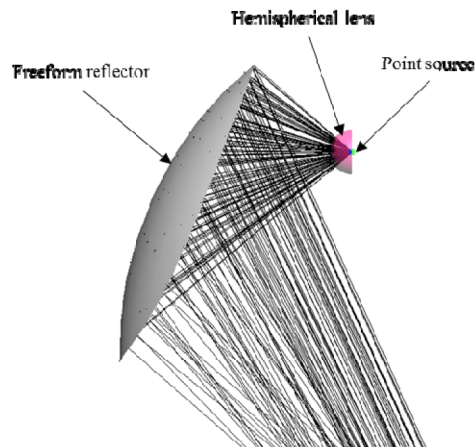


Fig. 5. A freeform LED light consists of a freeform reflector, a hemispherical lens, and a point source LED. The hemispherical lens collimates the Lambertian light emission from LED to a smaller radiation cone so that LED does not block the reflected light ray.

The configuration depicted in Fig. 5 is perfect for wall washing and accent lighting; both have been widely used to emphasize the content and attract the viewers' attention [10]. Moreover, in this configuration the light source is not positioned between the reflector and the task plane, indicating that it can avoid the problem of obstructed illumination.

The first example for this configuration is accent lighting, which is widely used in museums and exhibitions to draw viewers' attention to paintings, statues and wall decorations [10]. Here a 15° -tilted Lambertian light source is covered by a hemispherical lens and placed at 0.8m away from the target plane. The freeform reflector is used to illuminate uniformly a $2\text{m} \times 2\text{m}$ target area, as Fig. 6(a) shows. The dimension of the reflector is $\sim 40.2\text{mm} \times 37.2\text{mm} \times 13.8\text{mm}$; it is located at 25mm away from the light source. Figure 6(b) shows the resultant illuminance pattern. It is obvious that inside the $2\text{m} \times 2\text{m}$ region, the illuminance pattern is uniform and quickly drops to zero outside that region. Such illuminance pattern is ideal for accent lighting where only the content is illuminated and the background is dark so that the content stands out [11].

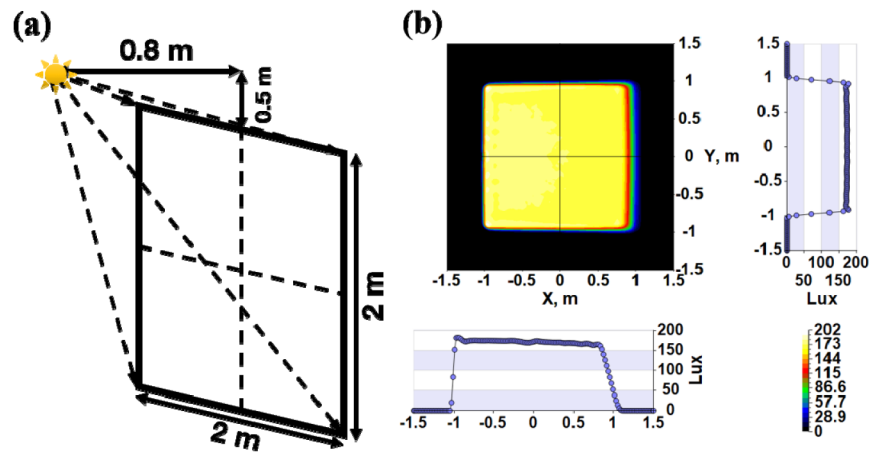


Fig. 6. (a) Illumination configuration of the freeform reflector for accent lighting, and (b) the simulated illuminance distribution on the target plane.

Another example is luminaires for large area wall washing. For these applications, a single luminaire is required to cover the entire height direction, while in the width direction an array of luminaires are set up to cover it all. In our design, we assume the height is along x-axis and width is along y-axis. For this task, we have designed a freeform reflector for large area wall washing. For a single luminaire, the configuration is the same as that shown in Fig. 6(a) and the luminaire can cover an area of $2\text{m} \times 2\text{m}$. However, this time the illuminance pattern is uniform along the x-axis (height), while in the y-axis (width), the illuminance has the triangular shape, as shown in Fig. 7(a). When the luminaires are aligned along the y-axis with spacing value Δy equals to or slightly less than 1m. Their borders along the y direction tend to disappear and we can get uniform illuminance pattern over a large area, as shown in Figs. 7(b)-7(d). Also from Fig. 7(b)-7(d) we can tell that such luminaires are not very sensitive to the spacing value Δy . This makes such freeform reflector ideal for large area wall washing. The reflector has a dimension of $\sim 39.2\text{mm} \times 39.4\text{mm} \times 13.5\text{mm}$ and is located 25mm away from the light source.

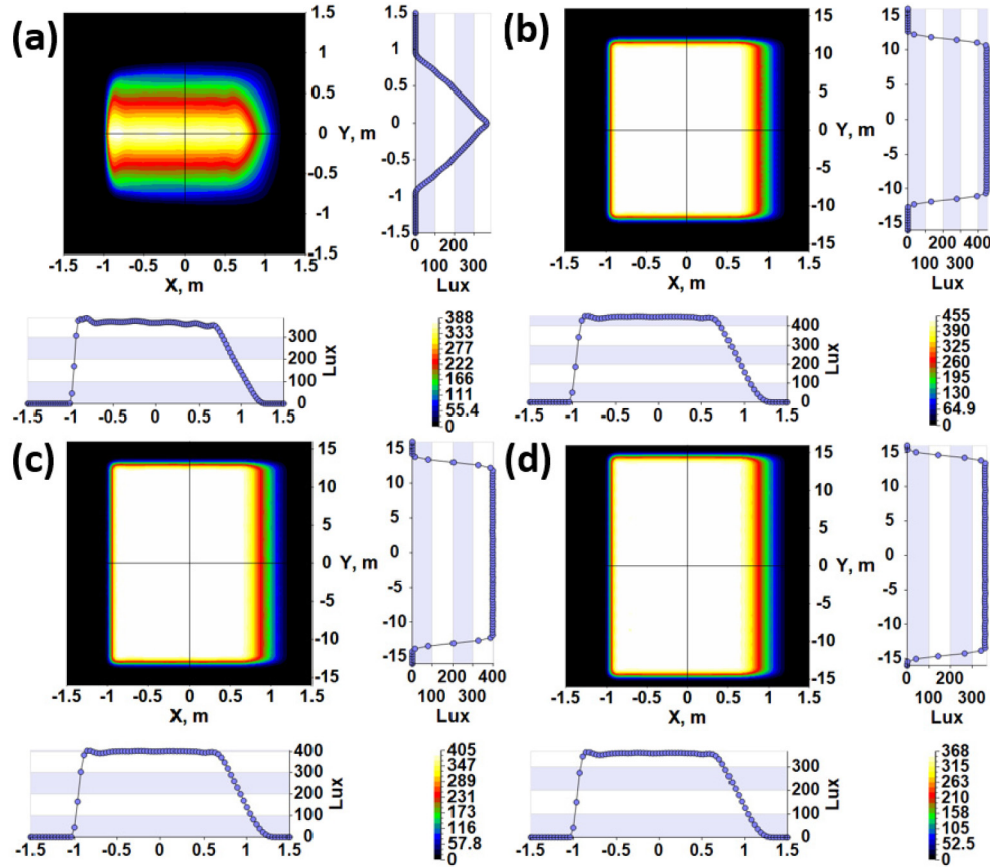


Fig. 7. (a) Illuminance pattern of a single freeform wall washer; using the wall washers for large area wall washing with different spacing value Δy in the y direction (b) $\Delta y = 0.8\text{m}$ (c) $\Delta y = 0.9\text{m}$ and (d) $\Delta y = 1.0\text{m}$.

4. Discussion

The Olikier's algorithm is based on the point source assumption, whereas in real world most of light sources are extended. Freeform optics is usually very sensitive to system modifications [26]. To understand the effect of extended sources, we replace the light source for accent lighting with real LEDs with Lambertian emission pattern. Then we place a hemispherical lens on top of the LEDs to confine their emitting cone. First, we replace the point source with CL-194S-WS, whose packaging is shown in Fig. 4(a). We can see that there is not much change in terms of illuminance pattern [Fig. 8(a)]. This is because the whole packaging of CL-194S-WS is $1.6\text{mm} \times 0.8\text{mm} \times 0.3\text{mm}$, which is quite small as compared to the dimension of the freeform reflector for accent lighting. However, if we replace the point source with a Cree CXA2011 light source in Fig. 8(b), whose dimension is $\phi 16.2\text{mm}$ for the LED chip and $22\text{mm} \times 22\text{mm} \times 2.275\text{mm}$ for the whole packaging, we can find in Fig. 8(c) that the sharp illuminance cutoff at the four edges has vanished, leaving smooth long "tails" at the edge. In accent lighting, this means if the target is still $2\text{m} \times 2\text{m}$, there will be a gradual illuminance drop across the target, and the luminaire will naturally cast a shadow on the background [10–12]. All of these will de-emphasize the target. As for large area wall washing, if we replace the point source with Cree CXA2011 [result shown in Fig. 8(d)], in the x-axis the same problem as the freeform reflector for accent lighting exists. While in the y-axis, we can still get uniform illuminance. Luckily, for large area wall washing, the

requirement for illuminance along the height direction (x-axis) is usually less strict compared to the requirement for accent lighting [10–12].

A possible solution for the extended source is to increase the relative size/distance between the real light source and the freeform reflector; this will make the extended source more “point-like”. A further improvement is to add illuminance compensation algorithms [21, 27, 28] for the reflector design.

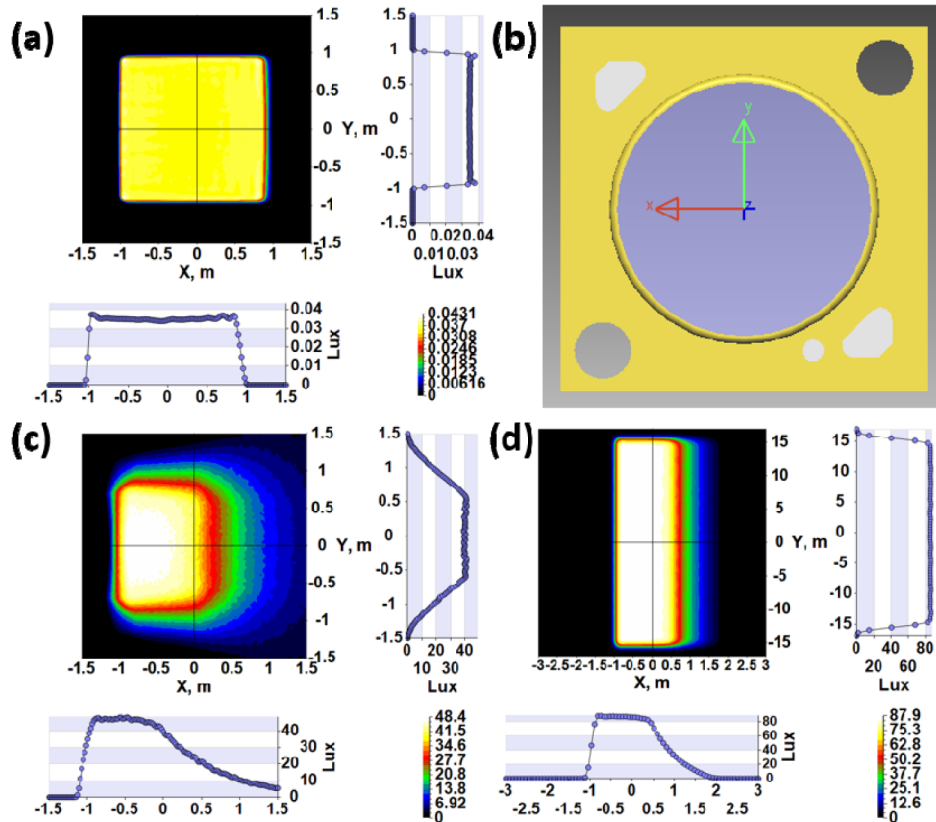


Fig. 8. (a) Illuminance pattern of the freeform reflector for accent lighting when the point source is replaced by CL-194S-WS. (b) The packaging of Cree CXA2011. (c) The illuminance pattern of the freeform reflector for accent lighting when the point source is replaced by Cree CXA2011. (d) Using Cree CXA2011 for large area wall washing with an array of freeform reflectors designed for large area wall washing.

5. Conclusion

With the abovementioned examples, we have proved that our improved design method is sufficient for design freeform reflectors for architectural lighting. These reflectors work well for accent lighting and large area wall washing. These design concepts can be extended to other architectural lighting applications such as wall grazing and cove lighting.

Acknowledgments

The authors are indebted to Prof. Vladimir Oliker from Emory University for the insightful discussion about the Oliker’s algorithm, Dr. Cristina Canavesi from LightTopTech for useful discussion about the intersection calculation method, Guanjun Tan for useful discussion about Monte Carlo ray tracing, and AFOSR for partial financial support under contract No. FA9550-14-1-0279.